Cement and Concrete Composites 140 (2023) 105083

Contents lists available at ScienceDirect

Cement and Concrete Composites

journal homepage: www.elsevier.com/locate/cemconcomp

Impact of humidity and vegetable oil addition on mechanical properties and porosity of geopolymers

Yunus Seyrek [a], Ognjen Rudic [a], Florian Mittermayr [a,*], Cyrill Grengg [b], Bernhard Freytag [c], Joachim Juhart [a]

[a] Institute of Technology and Testing of Building Materials, Graz University of Technology, Inffeldgasse 24, 8010, Graz, Austria
[b] Institute of Applied Geosciences, Graz University of Technology, Rechbauerstraße 12, 8010, Graz, Austria
[c] Laboratory for Structural Engineering, Graz University of Technology, Inffeldgasse 24, 8010, Graz, Austria

ARTICLE INFO

Keywords:
Geopolymer
Curing
Vegetable oil addition
Mechanical performance
Pore size distribution

ABSTRACT

In this study, the effects of humidity and vegetable oil addition (3.6 wt% of the total mix) on the mechanical and microstructural properties of metakaolin-slag-based geopolymer materials were studied. Oil addition resulted in a significantly modified porous microstructure, dramatically reducing the specific inner surface as well as the gel and capillary porosity of the materials. Most importantly, this modification mitigated negative effects on material properties induced by desiccation. Results were used to adopt the fib Model Code from 2010 to obtain predictive values for mechanical properties for geopolymer materials which are essential for the design of composite structures with normal concrete. The promising results from this study may contribute to solving other well-known weaknesses of geopolymers, such as high drying shrinkage and other diffusion-related (durability) issues. These new findings highlight the potential of geopolymer-vegetable oil composites as a future high-tech and low-carbon construction material.

1. Introduction

Geopolymers (GPs), often referred to as alkali-activated materials (AAM), are alternative binder materials that are considered to be more environmentally friendly compared to ordinary Portland cement (OPC) based building materials. While the ecological benefits of GPs are still under debate, they are especially known for their high-temperature resistance and high durability in environments exhibiting challenging (bio)chemical conditions, e.g. sewer systems or biowaste facilities [1–7]. The reasons, therefore, are the distinct structure and chemistry of the microstructural framework of GPs, which is strongly divergent compared to OPC systems.

Its particular durability properties suggest a high potential for GPs to be used in (bio)chemically aggressive environments for new structures or as repair mortars [8]. Envisaged future applications are composite construction of GP-OPC precast elements or GP repair for OPC-concrete structures. Advanced knowledge of material characteristics is required in order to achieve a strong bond between the different materials [9]. In particular, the evolution of the mechanical properties over time of the bonded materials is crucial during their hardening. However, the application of GPs for composite construction is still limited because of a lack of design guidelines [10]. Moreover, GPs are known to strongly respond to variable humidity conditions resulting in considerably higher drying shrinkage rates compared to OPC [11–16]. This can lead to constraint stresses and cracks, especially if hindered by a bond with other materials (usually OPCC). The most relevant factors controlling the bond between two materials are autogenous and drying shrinkage, compressive strength (CS), splitting tensile strength (STS) and the development of the modulus of elasticity (MoE). Besides compositional aspects, described parameters can be strongly influenced by the applied curing procedures. For instance, several studies showed that heat curing applied on GP materials increased the reaction kinetics during the polymerization process [17–22]. This impacted the final material properties such as mechanical strength and the corresponding porous microstructure. Additionally, a recent study by Hasnaoui et al. [23] reported that hardening at 50% relative humidity (RH) led to higher porosity and decreased mechanical performance compared to wet curing. However, very few systematic studies are available on the effect of relative humidity during curing on the development of the overall physical and microstructural properties of GPs. In this context, the associated porous microstructure strongly impacts the material

* Corresponding author.
E-mail address: f.mittermayr@tugraz.at (F. Mittermayr).

https://doi.org/10.1016/j.cemconcomp.2023.105083
Received 30 November 2022; Received in revised form 15 March 2023; Accepted 16 April 2023
Available online 17 April 2023

Abbreviations

BET	Brunauer-Emmett-Teller
BJH	Barrett–Joyner–Halenda
CEB-FIB	fib Model code 2010
CS	compressive strength
DVS	dynamic vapour sorption
GGBFS	ground granulated blast furnace slag
GP	geopolymer
GPM	geopolymer mortar
GPM-O	geopolymer oil mortar
GPM-S	geopolymer mortar-sealed
GPM-U	geopolymer mortar-unsealed
GPM-O-S	geopolymer mortar oil-sealed
GPM-O-U	geopolymer mortar oil-unsealed
M	moisture content
MoE	modulus of elasticity
MSA	metakaolin/slag-based aluminosilicate precursor
OPC	ordinary Portland cement
OPCC	ordinary Portland cement concrete
OPCM	ordinary Portland cement mortar
OPCM-S	ordinary Portland cement mortar-sealed
OPCM-U	ordinary Portland cement mortar-unsealed
PSD	pore size distribution
r_e	evaporation rate
RH	relative humidity
s	coefficient for the effect of the binder
S	sealed
S_p	specific surface
STS	splitting tensile strength
T	temperature
U	unsealed

response, ultimately controlling shrinkage, strength development and thus overall engineering properties [24–28].

Accordingly, a detailed and systematic understanding of relevant curing conditions, and the influence of desiccation together with other measures to control drying shrinkage, such as compositional material modifications, are therefore particularly useful to guarantee the required bond between GPs and normal concrete in composite elements. One interesting compositional additive, potentially impacting the physicochemical material properties of GPs, is (vegetable) (waste) oil. Investigations on the utilization of industrial waste oil (e.g. engine and vegetable) in small quantities (0.075–0.30 [29] and 0.6–1.7 wt% per binder [30]) in OPC showed increasing freeze-thaw resistance and a decreasing drying shrinkage rate without significantly compromising the final CS. The former was attributed to the introduction of large spherical pores by oil. Whereas the latter was attributed to a lower rate of water absorption by capillarity, saturation coefficient, and surface energy compared to specimens without oil [31]. Nevertheless, the stabilization of oil in OPC significantly retarded the setting and oil did not form strong chemical bonds with the cementitious matrix [32].

Little knowledge exists regarding the detailed effects of oil addition in GPs to adjust physicochemical material properties. So far, research focused on the production of highly porous GP foams using vegetable oils by an emulsion templating method [33–36]. Therein, alkanoic acids of the vegetable oil produce surfactants in highly alkaline media resulting in saponification processes. This progression reduces the interfacial tension between oil and the aqueous phase resulting in an interconnected ultra-macro-porosity within the hardened GP matrix. Heat curing (T > 800 °C) was then applied in the former studies to extract oil-based products from the GP matrix to obtain GP foams [32].

In this study, the impact of humidity and vegetable oil addition on critical physicochemical material properties such as porosity, strength development and modulus of elasticity was systematically investigated and subsequently compared to formulations without oil addition. Results were correlated to values obtained for standard OPC, in order to understand the implications for the development of GPs. Obtained mechanical data was used for predictive calculations over time-based on existing models for OPC materials and adopted for GP materials.

2. Materials & methods

2.1. Specimen preparation and curing conditions

The chemical compositions of the tested OPC and the metakaolin/slag-based aluminosilicate precursor (MSA) are presented in Table 1. As an activator, a potassium-based silicate solution (waterglass) with 35 wt % water content and a SiO_2/K_2O molar ratio of 1.92 was used. The aggregate used was 0/4 mm dry quartz sand. Geopolymer mortars (GPM), geopolymer-oil mortars (GPM-O), and reference ordinary Portland Cement mortars (OPCM) were prepared according to the mixture proportions listed in Table 2. The water content in the GPM-O mixture was decreased and partially replaced by sunflower oil. The paste volume (430 l/m^3) was kept constant in all mixtures. Flowability was measured according to EN 1015-3 [37]. 40x40 × 160 mm prismatic specimens were prepared and stored under 99% RH and 20 °C until demoulding. Since GPMs gain higher early strength than OPCM, a demoulding time of 3h was chosen for GPM and GPM-O and 24 h for OPCM. After demoulding, two curing conditions were applied as follows: (i) sealed conditions (S) covering specimens with plastic foil and storing them at 99% RH and 20 °C, and (ii) unsealed conditions (U) storing specimens at 65% RH and 20 °C without cover. A schematic description of the curing conditions and testing protocol is presented in Fig. 1.

2.2. Mechanical tests

The CS, STS and MoE tests of GPM and GPM-O were performed at 0.25 d, 1 d, 3 d, 28 d, and 91 d. For OPCM, these tests were performed at the same time intervals except 0.25 d (due to the demoulding time). Three specimens each were used for the mechanical tests. The CS and STS tests were conducted in accordance with EN 1015-11 [38] and EN 12390-6 [39], respectively. The MoE test was conducted on a universal testing machine, with a maximum 100 kN load cell capacity and a 1600 N/s loading rate by Austrian Standard ONR 23303 [40]. Two linear variable differential transformers (LDVTs) with 0.1% accuracy were used to measure the displacement. For sealed specimens, the plastic cover was not removed to avoid desiccation during the test.

Table 1
Chemical compositions of OPC and MSA [%].

	SiO_2	Al_2O_3	Fe_2O_3	CaO	MgO	MnO	TiO_2	Na_2O	K_2O	SO_3	P_2O_5
OPC	19.77	4.39	3.17	62.20	2.78	0.18	0.27	–	0.83	3.25	0.21
MSA	32.04	24.99	25.21	7.78	1.71	0.37	3.17	0.36	0.15	0.22	0.14

Table 2
Mixture proportions [kg/m^3].

	CEM I 42.5 N	water- glass	MSA	vegetable oil	water	Sand 0/4	SP[a]	w/s[b]	l/s[c]	w/c[d]	flow [mm]
OPCM	557.2	–	–	–	248.8	1504	1.7	–		0.45	171
GPM	–	269.5	399.7	–	120.8	1504	–	0.37	0.37	–	197
GPM-O	–	235.7	349.6	78.80	73.40	1504	–	0.31	0.47	–	113

[a] Superplasticizer.
[b] Total water/solid (total water = Σadded water + water content of water glass; solid = ΣMSA + solute content of water glass).
[c] Liquid/solid (liquid = total water + oil).
[d] Water/cement.

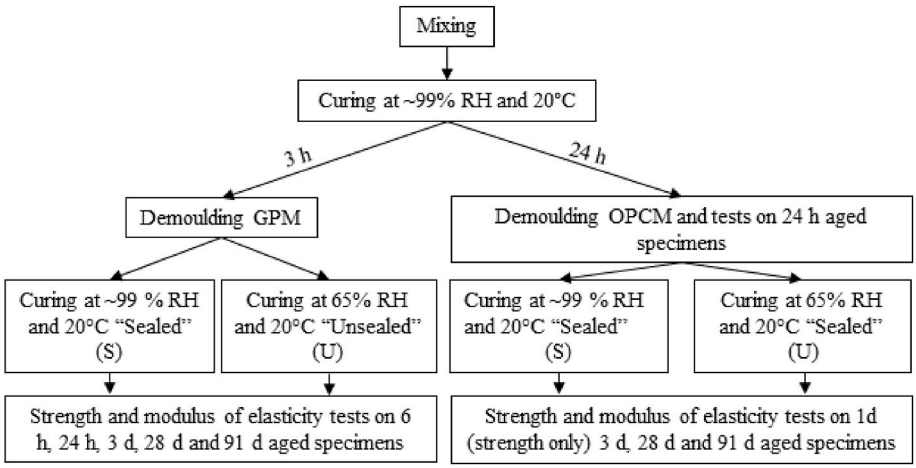

Fig. 1. Workflow diagram.

2.3. Moisture content

After the MoE tests, the moisture content M, of each specimen was determined according to Equation (1) where m_I is the dried weight at 105 ± 1 °C after 25 h (the mass change <0.2%) and m_o is the initial mass after demoulding.

$$M = \frac{m_I - m_o}{m_o} \cdot 100 \tag{1}$$

2.4. Open porosity and pore size distribution

The open porosity was evaluated in accordance with EN 1936:2007 [41]. Additionally, nitrogen (N_2) adsorption and Dynamic Vapor Sorption (DVS) methods were applied on prism specimens after 7d of curing at ~99% RH and 20 °C to characterize the porous microstructure between 2 and 100 nm. In order to preserve the microstructure of the OPCM specimens, the solvent-exchange method (immersion in isopropyl alcohol for two weeks and then vacuum drying for one week) was adopted [42]. No stoppage procedure was used for the geopolymer specimens, as it might change the pore structure [43]. Therefore, only vacuuming for BET on the day of testing was used and no further preparation in the case of DVS to preserve the fine gel pore structure as well as possible. No temperature treatment was applied in order to avoid alterations to the initial porous microstructure. N_2 sorption isotherm experiments were carried out at 77K temperature. Approximately 1g of the mortars was gently chopped and vacuumed down to 10 Pa for 24h to remove the moisture. Based on the N_2 adsorption data, the Barrett–Joyner–Halenda (BJH) model was used to derive the pore size distribution (PSD) curve of the adsorption isotherm branch [44], while the Brunauer-Emmett-Teller (BET) model [45] was applied to calculate the specific surface (S_p) of the materials. DVS analyses were conducted by the dynamic water vapour sorption analyzer (GraviSorp 120, Porotec) device. Adsorption and desorption isotherms were obtained at 25 °C and at RH levels ranging from 94 to 1%, with an airflow of 1 m/s. The moisture content of the specimen at equilibrium at each relative humidity was expressed as a mass of water per mass of dry material. As in the case of N_2 adsorption analysis, the BJH and BET models were used to evaluate PSD and S_p values. Pore sizes (pore diameters, D_p, in nm) of the investigated materials were categorized in three pore size ranges: Pores within the pore diameter ranges of 2–10 nm, 10–20 nm and 20–100 nm, corresponding to gel, small capillary and medium capillary pores, respectively [46].

2.5. Mathematical description of mechanical properties over time

The evolution of mechanical properties over time as an important design characteristic was first calculated according to the equations of the fib Model code 2010 (CEB-FIB) [47]. Therein, the strength evolution is predicted by Equation (2) using the 28d CS, f_{cm} (MPa) and a function, β_{cc} according to Equation (3) depending on the time t (days). Here, s is an empirical coefficient that represents the effect of the binder [47]. For OPC, s is particularly influenced by the cement type and its strength class ($s = 0.20$ at $f_{cm} \geq 60$ MPa for OPC).

$$f_{cm}(t) = \beta_{cc}(t) \cdot f_{cm} \tag{2}$$

$$\beta_{cc}(t) = \exp\left\{ s \left[1 - \left(\frac{28}{t} \right)^{0.5} \right] \right\} \tag{3}$$

The MoE (MPa) for concrete at an age t (days) was estimated by the following Equation (4) and (5):

$$E_{ci}(t) = \beta_E(t) E_{ci}$$

with

$$\beta_E(t) = [\beta_{cc}(t)]^{0.5} \tag{4}$$

$$E_{ci} = E_{co} \cdot \alpha_E \cdot \left(\frac{f_{cm}}{10}\right)^{1/3} \quad (5)$$

E_{ci} is the MoE (MPa) at an age of 28d, $\beta_E(t)$ is a coefficient that depends on the age (days) of the concrete, $\beta_{cc}(t)$ is the coefficient according to Equation (3), E_{co} is a given value of 21500 (MPa) for OPCC, α_E is the aggregate coefficient (α_E=1 for quartz aggregates) and f_{cm} is the mean CS (MPa) [47].

3. Results

3.1. Compressive strength and splitting tensile strength

The effect of desiccation prevention on the development of CS and STS is presented in Fig. 2a and b, respectively. Regardless of the curing condition and oil addition, at a very early age (0.25d) all GPM and GPM-O specimens exceeded a CS of 30 MPa while OPC specimens exhibited a much lower strength (not demoldable) (Fig. 2a). After 1d, all GPMs gained more than 75% of their 28d CS. Unlike GPM, OPCM had a more gradual increase of CS with time and reached higher overall CS values. The different curing conditions caused clear variations in the CS evolution of the GPMs. Under sealed (S) condition (99% RH) specimens showed a gradual strength increase (after an initial high gain in strength) with time reaching the highest strength after 91d (GPM-S). In contrast, there was no significant gain in CS after the first day when stored at 65% RH (GPM-U). The addition of oil resulted in a continuous gain in CS after 1d even at 65% RH. Both series with oil, GPM-O-S and GPM-O-U, developed a gradual CS increase reaching similar final values. Nevertheless, these final values were 17% lower than the final 91d-strength specimens without oil cured at 99% RH (GPM-S).

Similar trends were observed for STS (Fig. 2b). All GPM specimens revealed a higher early strength compared to OPCM. After 91d GPM-S specimens reached similar STS values as OPCM (S & U) (GPM-S = 5.6 MPa; OPCM-S = 5.6 MPa and OPCM-U = 5.4 MPa). Unsealed curing conditions significantly reduced the final STS values of GPMs by up to 36%. Oil addition led to overall reduced STS values of roughly 30% after 91d. However, slightly increase early strength values were observed. Interestingly, no relevant difference in STS evolution was found when comparing the two oil series (S & U).

3.2. Modulus of elasticity

The MoE test results of OPCM, GPM and GPM-O under the two different desiccation conditions are presented in Fig. 2c. OPCM had similar MoE behaviour regardless of the desiccation condition. On the contrary, the MoE for GPM-S was ~30% lower compared to the OPCM. For the GPM series, in general, there was a great increase in the MoE in all series from 0.25d to 1d for both desiccation conditions. GPM-S increased up to 28d, whereas no significant increase was observed for the GPM-U after 1d. The unsealed desiccation condition drastically affected the overall performance of GPM-U, so the final MoE was even 30% lower than GPM-S. The addition of oil resulted in a slightly increased MoE for both desiccation conditions within the first 3d. It was observed that oil addition increased the MoE with time for both conditions. While GMP-O-S had a slightly lower 91d MoE (4.9%) than GPM-S, GPM-O-U reached similar values resulting in a 30% higher ultimate MoE compared to GPM-U.

3.3. Evaluation of compressive strength and modulus of elasticity over time

The CS values of OPCM and GPM under different curing conditions and their corresponding functions over time, are calculated based on Equation (2) and (3) and plotted in Fig. 3a. For OPC based concrete the empirical coefficient s reflects the strength development over time depending on the cement type [47] (lower s indicates a higher strength

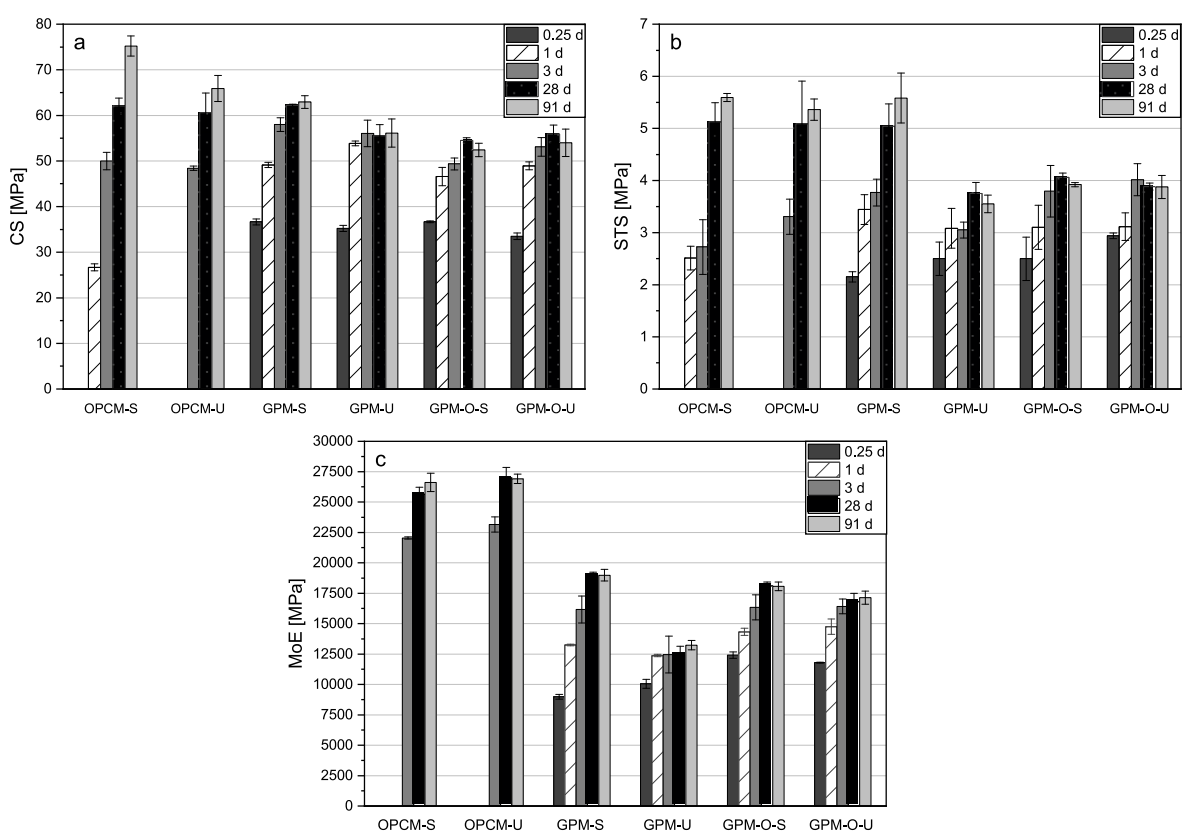

Fig. 2. Effect of curing conditions on (a) the compressive strength, (b) the splitting tensile strength and (c) the modulus of elasticity.

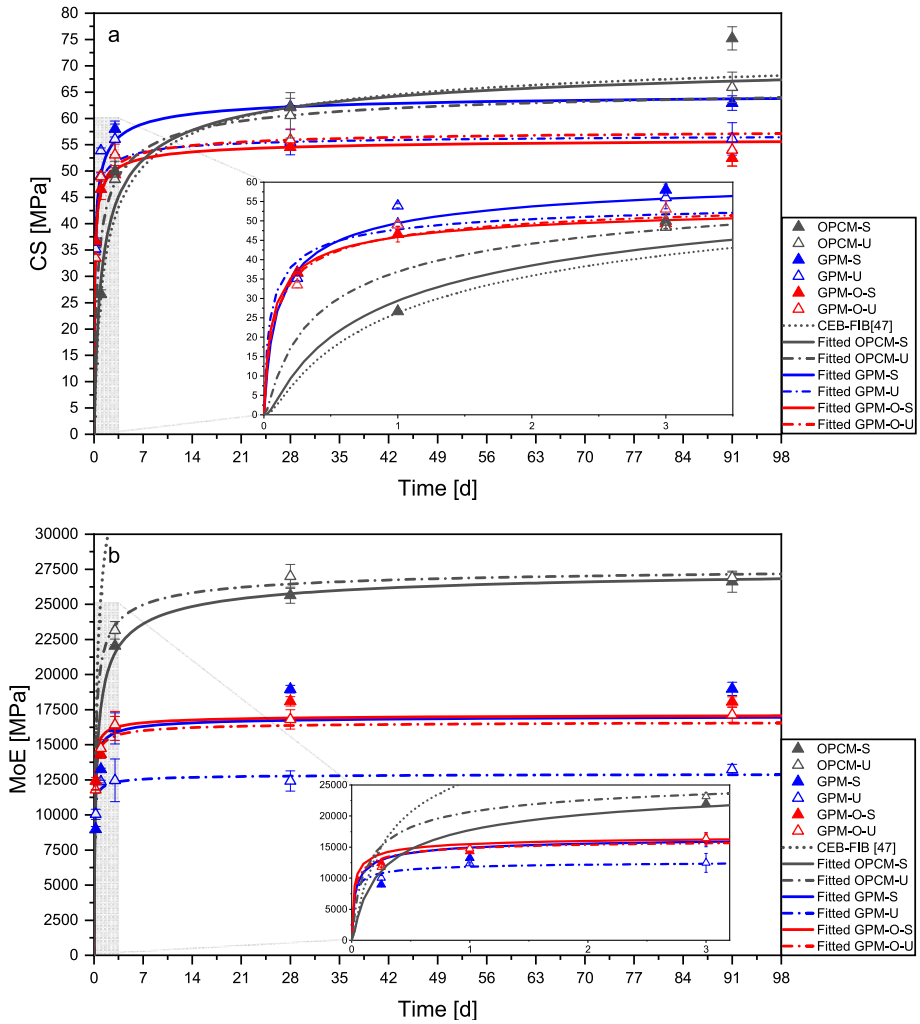

Fig. 3. Comparison between measured and predicted (a) compressive strength and (b) modulus of elasticity.

development [48]). For the investigated specimen series, s was adopted by regression analysis based on Equation (2). The derived s-coefficients and corresponding high regression coefficients (R^2) are presented in Table 3. The absolute difference between the s coefficients of curing conditions (sealed-unsealed) of each mixture is also shown (Δs).

The MoE development over time according to the CEB-FIB code [47] is plotted in Fig. 3b. Additionally, curve fitting on basis of Equation (4) and (5) was applied with the factor $E_{co}.\alpha_E$ as a variable. For OPCM-S and OPCM-U coefficient $E_{co}.\alpha_E$ was identified as 14015 and 14510 MPa, respectively. Furthermore, for GPM-S, GPM-U, GPM-O-S and GPM-O-U $E_{co}.\alpha_E$ was found as 9104, 7210, 9603 and 9302 MPa, respectively. All calculated predictions are in good agreement with the experimental data ($R^2 \geq 0.90$).

Table 3
Derived s coefficients, regression coefficients (R^2) and absolute difference of s between sealed and unsealed specimens (Δs).

	s	R^2	Δs
CEB-FIB [47]	0.2000	–	–
OPCM-S	0.1742	0.98	0.0587
OPCM-U	0.1155	0.99	
GPM-S	0.0536	0.99	0.0187
GPM-U	0.0349	0.96	
GPM-O-S	0.0404	0.99	0.0053
GPM-O-U	0.0457	0.98	

3.4. Change in moisture content

The change in moisture content with time is presented in Fig. 4. The initial absolute values, which were calculated based on the mixture

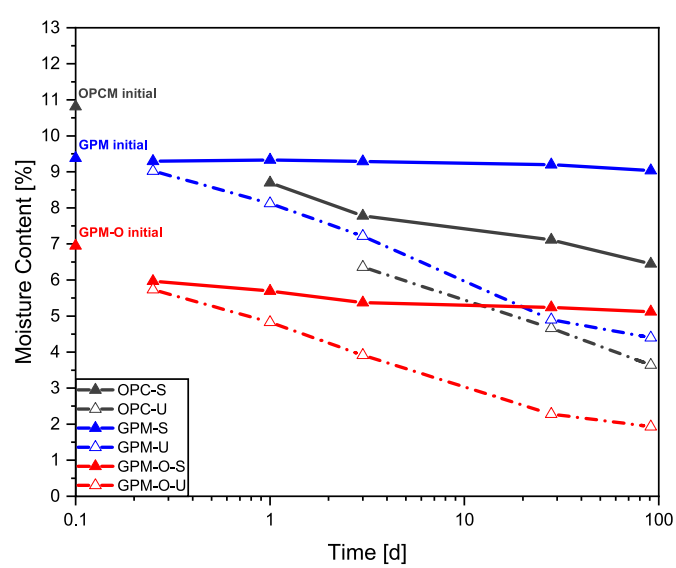

Fig. 4. Moisture content change over time.

proportions, were 10.8, 9.4 and 7.0 wt% for OPCM, GPM and GPM-O, respectively. For the OPCMs the moisture content dropped gradually over time. At 91d OPCM-S had lost ~40% of its moisture and OPCM-U ~66%. The different curing led to a relative reduction of ~44% when comparing sealed to unsealed curing at 91d. Compared to the initial moisture content, the values for GPM-S only slightly decreased until 91d. The trend was the same for the GPM-O-S from 0.25d to 91d. Interestingly, between the initial and the 0.25d values a difference of ~14% was observed for the GPM-O series. Unsealed specimens exhibited less than half of their initial moisture content after 91d (GPM-U lost 53%, GPM-O-U lost 72%).

3.5. Porous microstructure

Similar open porosity values (19.4 ± 0.6%) were measured for OPCM and GPM sealed and unsealed mortars at the age of 7 d (Fig. 5a). On the contrary, a significant reduction of the total open porosity down to 8.6% and 11.2% were measured for GPM-O-S and GPM-O-U, respectively.

Considerable higher S_p values (Fig. 5b) in the case of GPM specimens were observed compared to OPCM and GPM-O specimens. The notable differences of measured S_p values between DVS and N_2 adsorption methods (for example 23.6 m^2/g vs. 9.1 m^2/g in case of OPCM-S) occurred due to better accessibility of water molecules than N_2 molecules [49]. Different trends of the S_p values of unsealed and their sealed counterparts were also observed (i.e. a slight increase of S_p values in comparison to their slight decrease in the case of GPM and OPCM (Fig. 5b) which may be ascribed to the mentioned differences in accessibility of water and N_2 molecules, i.e. the existence of some N_2-inaccessible regions.

The addition of oil led to a substantial decrease in porosity. The open porosity was much lower and also the S_p values of GPM-O in comparison to GPM were dramatically reduced (Fig. 5b). The PSD revealed this porosity reduction is mainly stemming from a notable decrease of the gel and capillary porosities i.e. pore diameters up to 30 nm (Fig. 6). It is shown that PSD for GPM-S and GPM-U have two distinctive peaks while PSDs of GPM-O-S and GPM-O-U show only one peak.

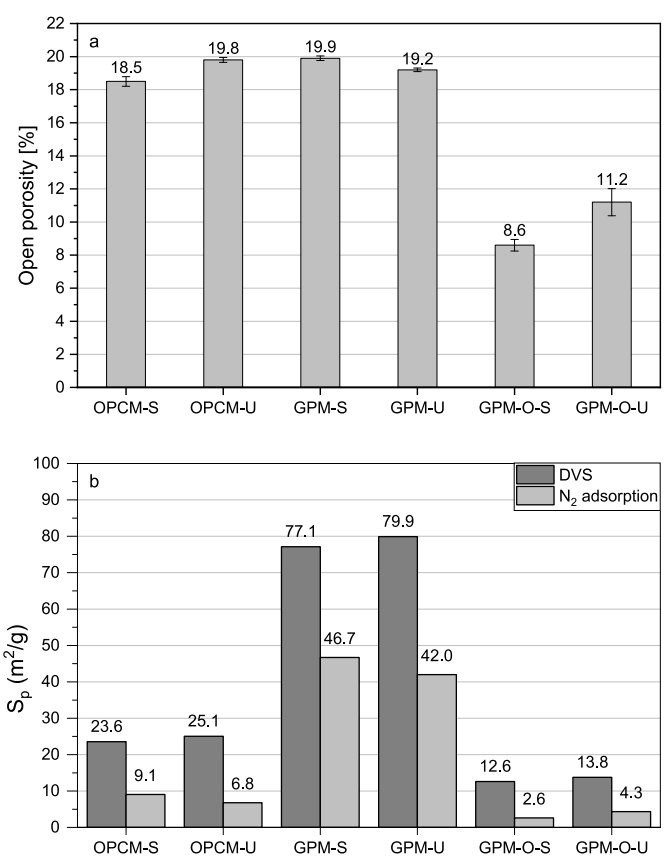

Fig. 5. (a) Open porosity measurements at 7d and (b) specific surface evaluated by N_2 adsorption and DVS.

4. Discussion

4.1. Impact of the desiccation protection on mechanical and physical properties of GPM

The strength test results show that the curing conditions strongly affected the GPMs' (without oil) strength development over time, whereas a significantly lower impact was found for the OPCM. This is in accordance with previous findings reported in the literature [23,50]. If the sealing is not sufficient or strength development is slow, a fast loss of this unbounded water during hardening causes drying shrinkage, microcracking and reduced reaction degrees. The high early strength of the GPM is associated with the polymerization process exhibiting fast reaction kinetics [51], whereas the pronounced increase of strength until 91d, is mainly attributed to the hydration of slag particles in the GPMs [51]. Fast drying due to unsealed curing conditions causes an incomplete latent-hydraulic reaction of components such as GGBFS, thereby decreasing the potential strength of GPMs [23]. This is also clearly reflected in the results, where no further increase in strength was recorded after 24h for the unsealed GPM specimens. The results of GPM-O showed that the strength development of specimens with oil was practically unaffected by the curing conditions. The measured moisture contents confirm the strength results. Obtained water decrease at low rates in the sealed GPM is most likely related to the hydration of GGBFS in the mixtures [52]. The observed moisture loss of ~40% of OPCM-S under sealed condition can be explained by ongoing hydration [52].

A similar pattern for strength is obtained for the modulus of elasticity results, where a great variance of sealed and unsealed GPM was observed (Fig. 2). Within the first 24 h, the development of the modulus of elasticity is similar in both series (reaching roughly 12500 MPa), while no further increase could be measured thereafter for the GPM-U specimens. The modulus of elasticity of GPM-S in contrast gradually increased and reached around 19000 MPa after 91 d. Similar to OPC-based materials, the curing of GPs containing GGBFS at high RH, enables a higher hydration degree, associated with a denser microstructure, a shift in porosity (Fig. 6b) and a higher modulus of elasticity [53,54]. Note that early age MoE (0.25d, 1d) of GPM was remarkably higher than that of OPCM. GPM-O developed a significantly higher MoE than GPM without oil at early ages (0.25d and 1d), indicating that the oil addition causes higher early stiffness.

Described variations in mechanical properties are supported by the observed changes in the porous microstructure between the materials cured at different RH conditions. In specimens exposed to unsealed conditions capillary water diffusion from the interior of the material to the surface is triggered, while in the case of sealed conditions such capillary diffusion and consequently evaporation is hindered. The water diffusion towards the surface induces internal pressure generated by the surface tension of the pore solution, causing a modification of the PSD of the material. Different curing conditions affect the diffusion of the water vapour in a dissimilar way, which then in turn influences the differences related to the porous microstructure (Fig. 6). The exposure to unsealed conditions shifted the PSD curve of GPM-U to smaller pore sizes in comparison to the PSD of GPM-S, with a certain alteration of gel porosity and a decrease of porosity in the capillary pore sizes range. Such capillary stress-induced pore modification due to different curing conditions may additionally lead to partial redistribution of C-A-S-H and C–S–H phases resulting in different structural rearrangements [14,55].

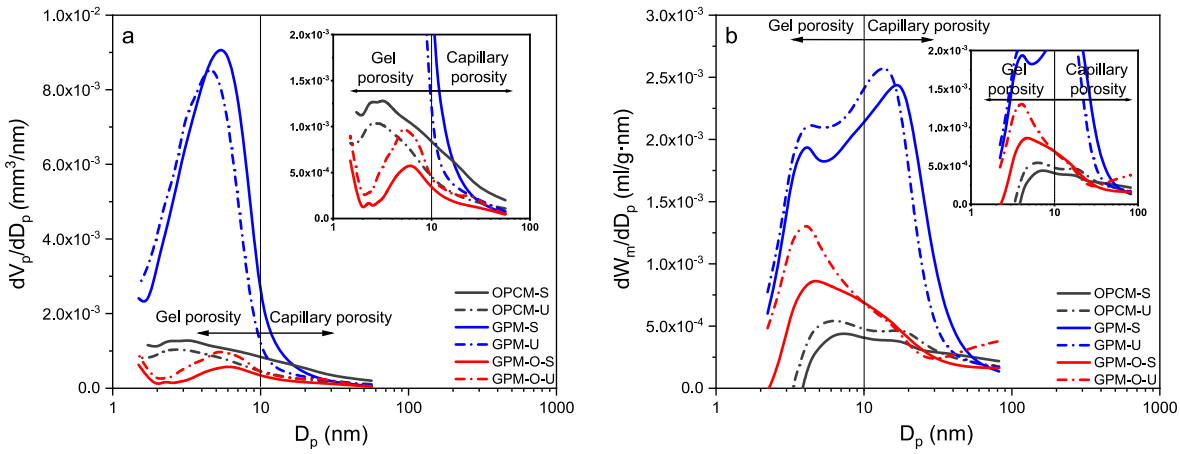

Fig. 6. PSD evaluation: (a) N_2 adsorption method; (b) DVS method.

4.2. Impact of oil addition and the response to different curing conditions

Oil addition (3.6 wt % of the total mix) significantly reduced the CS of GPM but not the MoE. The effect, that CS and MoE for GPs correlate differently compared to OPC is well known [56,57]. Furthermore, Duxson et al. [58] observed that more homogeneous matrices lead to higher MoE in GPs. During compression, the stress spread over a larger area resulting in less strain and higher MoE. In our case, the reduction in CS can be explained by entrained macro porosity [32]. The densification of the micro porosity and the widening of the macro porosity of the GPM observed here were oil-induced. However, there were no significant differences in strength when specimens were either sealed or unsealed. This is contrary to the GP specimens where no oil was added (GPM-S and GPM-U), as strength was much lower after unsealed curing (Fig. 2) due to desiccation. The relationship between the CS and the MoE of all data points is plotted in Fig. 7. Desiccation prevention by oil addition to GPM is visible as both CS and MoE were improved over GPMs where no oil was used.

It was also noted by Rocha et al. [59], that although metakaolin-based GPMs had similar CS values, the ones with denser microstructure (less porous) had a relatively higher modulus of elasticity. Accordingly, it can be concluded that the central parameter controlling the MoE is changing microstructural material properties resulting in a changed porous microstructure. The addition of oil, strongly reduced the open porosity and S_p of the GPM materials, thereby reducing the detrimental effects of unsealed curing conditions. However, small variations in the porous network structure between GPM-O specimens exposed to sealed and unsealed curing conditions could be observed. In comparison to GPM-O-S, both gel porosity and medium capillary pore size greater than 30 nm in diameter were slightly enlarged in the case of GPM-O-U indicating a minor impact due to higher water diffusion processes.

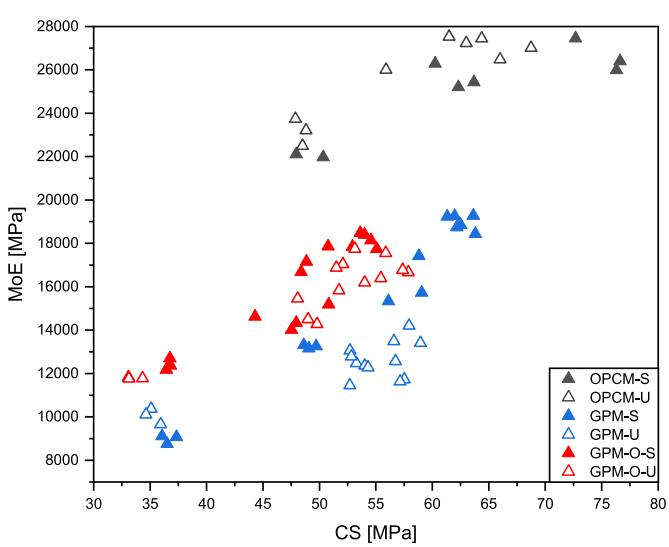

Fig. 7. Relationship between compressive strength and modulus of elasticity of all tested specimens.

To further evaluate the correlation between the different material properties, moisture content was plotted against STS and the modulus of elasticity (Fig. 8a and b). It can be seen in these figures that the ultimate STS of OPCM was in the same range for both curing conditions (grey area in Fig. 8a). In contrast, there is a significant difference between GPM-S and GPM-U. This difference in moisture content can be overcome with oil addition (red area in Fig. 8a). A similar trend is seen in Fig. 8b that the modulus of elasticity drops sharply for GPM-U, however, GPM-O-S and GPM-O-U have the same range of ultimate modulus of elasticity (red area in Fig. 8b) despite different moisture content. This strongly argues for the impact of microstructural framework density and porous microstructure on the development of STS and modulus of elasticity [33,60,61]. Additionally, oil and associated reaction products (metal soaps) reduced the kinetics of internal evaporation protection, especially within the first 3 days of curing, thereby increasing GGBFS hydration degrees at later stages.

4.3. Moisture transport properties during different curing conditions

From DVS data an evaporation isotherm versus time and RH can be derived (Fig. 9a). In that way, the porous microstructure of cement-based materials can be studied qualitatively, wherein different pore size categories are consequently separated in relation to different RH value ranges [62,63]:

- At the RH range of 94–70% - capillary pores and inter-hydrate spaces (i.e. the most refined capillary pores, similar size as the coarsest gel pores) are emptied,
- At the RH range of 70–40% gel pores are emptied,
- At the RH range of 40–5% water-filled spaces between interlayers are dried out.

Consequently, the evaporation rates (r_e, in mg/h) within 94%–70%; 70%–40% and 40%–5% RH value ranges were calculated from the slopes of the obtained evaporation isotherms Fig. 9a over time and presented in Fig. 9b.

The DVS analyses revealed notable similarities between evaporation isotherms and rates of evaporation (r_e) for the different curing conditions (Fig. 9). These findings suggest that water vapour evaporation

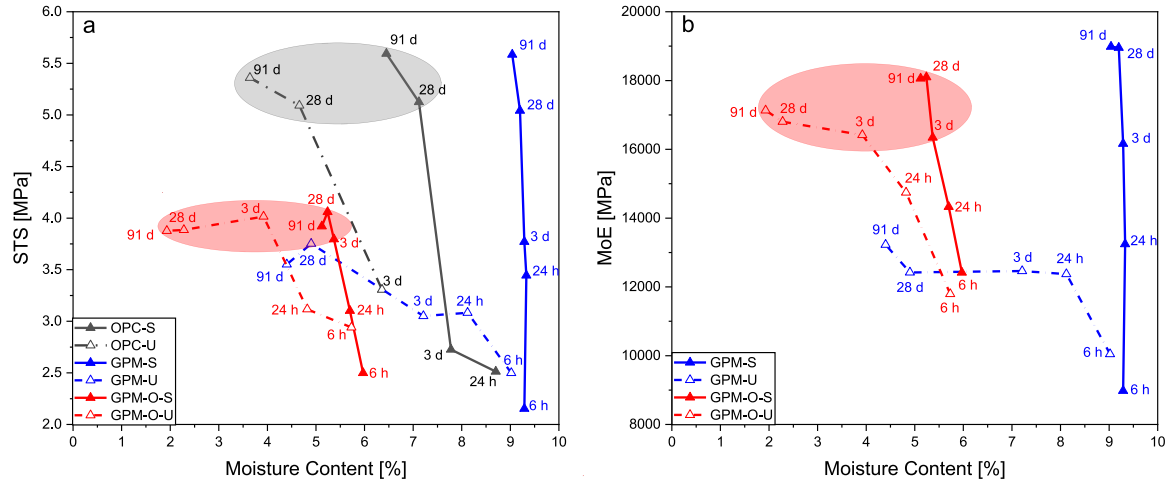

Fig. 8. (a) Moisture content-splitting tensile strength relationship, (b) moisture-modulus of elasticity relationship.

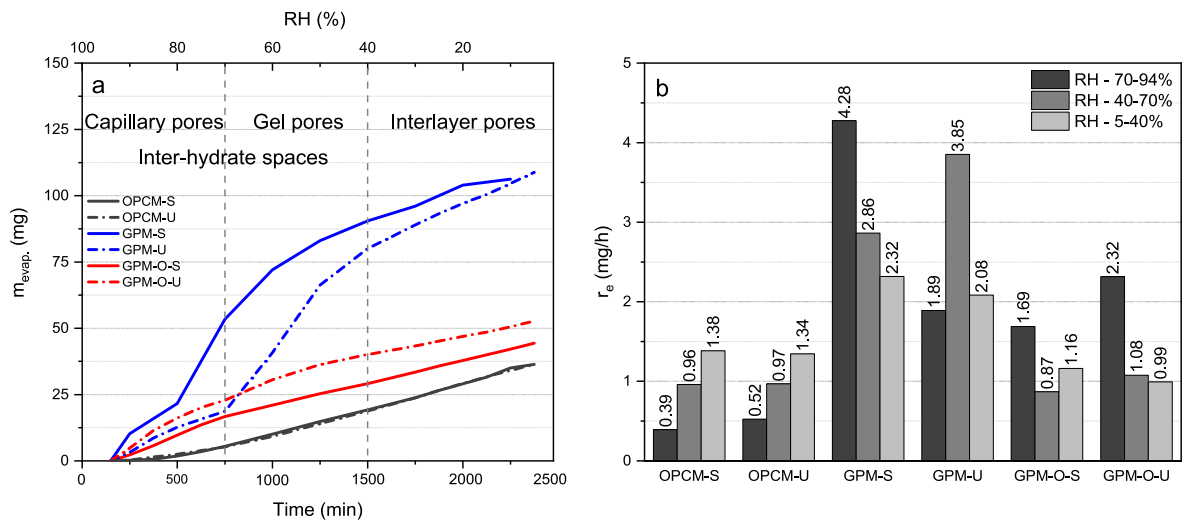

Fig. 9. (a) Evaporation isotherms versus time during the desorption cycles; and (b) rates of evaporation (r_e).

kinetics were not affected by changes in RH and by prior curing conditions for the OPC mortar specimens. In contrary GPMs showed different evaporation kinetics related to the surrounding humidity and curing conditions. In the case GPM mortars, the re value was found to be the highest (4.28 mg/h) in the range of 70–94% RH for sealed specimens (GPM-S). In case of unsealed specimens (GPM-U), the highest re value was 3.85 mg/h in the region of 70 - 40% RH. Sealing prevented capillary water diffusion from the interior of the material to the surface, therefore higher water retention within the capillary pores and the inter-hydrate spaces is likely responsible for the measured re value. These findings further confirm that sealed curing caused a coarser porous microstructure vs. unsealed curing during hardening (see also Fig. 6). During unsealed curing, water diffusion from the interior of the material occurred already during hardening. This resulted in a modified gel porosity and cause an overall reduction of capillary pore sizes (Fig. 6b). Consequently, a significant part of the capillary pores was already (partially) emptied during the hardening and framework formation of the GPs.

In the case of GPM-O, the evaporation isotherms and rate of evaporation transport were significantly lower in comparison to GPM (Fig. 9). The different curing conditions also resulted in a different trend of water vapour evaporation isotherms, but by far not as pronounced as for GPM. Contrary to the specimens without oil, GPM-O-S had a slightly higher re value at the high RH values compared to GPM-O-U. A reason for this could be the detected higher capillary porosity for the GPM-O-U (Fig. 6b) causing to some extent higher diffusion of water vapour through larger pores. The observed refinement of the gel and capillary porosities for GPM-O will also have an influence on the elastic modulus behaviour under different curing conditions. Notably lower amounts of gel and capillary pores (up to 80 nm) are most likely related to pore fillings with oil-related phases (metal soaps) [64]. These pore clogging contributed greatly to improving the stiffness and the toughness of such a composite material. When the small pores (≤80 nm) are less abundant, the microstructure gets densified, which then increased the modulus of elasticity [33,60,61].

4.4. Evaluation of mechanical properties over time

The presented findings show that it is possible to predict GPMs' CS development by modifying the *s* coefficient and using the functions proposed for OPCC from the CEB-FIB [47] (Fig. 3a). The *s* coefficient of 0.20 for OPCC had to be adapted to values of s~0.05 (0.03–0.05) for the GP-binder, indicating its higher early strength gain compared to OPC. The strength development and thus *s* coefficient was also influenced by unsealed curing. Whereas when oil was added, the type of sealing was no longer decisive, as Δ*s* was much smaller than for OPCM and GPM (Table 3). The fitted curves of both GPM-O series were very similar and

could be summarized by one identical fit (s = 0.05). The different curing conditions cause a significant variation between GPM-S and GPM-U, showing the effect of evaporation protection. In contrast, oil addition compensates for the lack of drying protection as no significant difference due to existing or non-existing sealing was found.

GPM's MoE over time can also be predicted by modifying the functions for OPC given in the CEB-FIB code [47] (Fig. 3b). $E_{co}.\alpha_E$ is adopted according to the *s* coefficients Table 3. In this study $E_{co}.\alpha_E$ coefficient was identified at approx. 14400 MPa for OPC mortars, while the CEB-FIB [47] code gives 21500 MPa for the used quartzite aggregates. This may be explained by the fact that the CEB-FIB code [47] is oriented towards concrete with a larger maximum grain size and higher content of aggregates compared to mortar, which greatly affects the (basic value of) MoE. The $E_{co}.\alpha_E$ coefficient decreases sharply when GPM-S (9104 MPa) and GPM-U (7210 MPa) are compared. In contrast, with oil addition, this coefficient does not change considerably (GPM-O-S: 9603 MPa and GPM-O-U: 9302 MPa) which is attributed to the desiccation prevention of oil addition. Finally, this study confirms that the MoE of GPs is generally lower than that of OPCs of the same strength class [65]. This can be related to the microstructural differences between the two systems.

5. Practical implications and concluding remarks

In this study, the impact of different curing conditions - namely sealed and unsealed - and the addition of vegetable oil on mechanical and microstructural properties of geopolymer (GP) mortars was experimentally investigated, modelled and compared to mortars based on ordinary Portland cement (OPC). The result of this study shows that:

- Limited effects of different curing conditions were observed for the OPC materials, while reduced relative humidity levels strongly impacted the mechanical and microstructural development of GP materials. Most importantly, this study shows that oil addition to GPs levels out negative effects on material properties invoked by the prevailing curing conditions.
- Oil addition positively enhances the modulus of elasticity and the early strength development regardless the curing conditions. This can be related to the significant microstructural modification caused by oil and its associated reaction products.
- Observed beneficial impact of oil is most likely not limited to the investigated strength development and the modulus of elasticity, but will also affect corresponding important material properties such as drying shrinkage and other diffusion related (durability) mechanisms.
- From an engineering and practical point of view, long known issues for geopolymers and alkali-activated-materials might be (partially) resolved by adding vegetable oil. Described improved material properties will enable enhanced bonding characteristics to normal concrete surfaces. This, in combination with excellent durability, might enable the use of geopolymers and alkali-activated-materials as future high-tech and low-carbon construction materials.

Declaration of competing interest

The authors declare that they have no known competing financial interests or personal relationships that could have appeared to influence the work reported in this paper.

Data availability

Data will be made available on request.

Acknowledgments

This research was financially supported by FFG in the frame of a Bridge project "BioResComp" (granted under NR. 871279 of Austrian research promotion agency FFG).

References

[1] M.A.M. Ariffin, M.A.R. Bhutta, M.W. Hussin, M. Mohd Tahir, N. Aziah, Sulfuric acid resistance of blended ash geopolymer concrete, Construct. Build. Mater. 43 (2013) 80–86, https://doi.org/10.1016/j.conbuildmat.2013.01.018.
[2] P. Duxson, J.L. Provis, G.C. Lukey, J.S.J. van Deventer, The role of inorganic polymer technology in the development of "green concrete, Cement Concr. Res. 37 (2007) 1590–1597, https://doi.org/10.1016/j.cemconres.2007.08.018.
[3] F. Aslani, Thermal performance modeling of geopolymer concrete, J. Mater. Civ. Eng. 28 (2016), 04015062, https://doi.org/10.1061/(asce)mt.1943-5533.0001291.
[4] C. Bai, P. Colombo, Processing, properties and applications of highly porous geopolymers: a review, Ceram. Int. 44 (2018) 16103–16118, https://doi.org/10.1016/J.CERAMINT.2018.05.219.
[5] F. Pacheco-Torgal, J. Castro-Gomes, S. Jalali, Alkali-activated binders: a review: Part 1. Historical background, terminology, reaction mechanisms and hydration products, Construct. Build. Mater. 22 (2008) 1305–1314, https://doi.org/10.1016/J.CONBUILDMAT.2007.10.015.
[6] C. Grengg, G. Koraimann, N. Ukrainczyk, O. Rudic, S. Luschnig, G.J.G. Gluth, M. Radtke, M. Dietzel, F. Mittermayr, Cu- and Zn-doped alkali activated mortar – properties and durability in (bio)chemically aggressive wastewater environments, Cement Concr. Res. 149 (2021), 106541, https://doi.org/10.1016/J.CEMCONRES.2021.106541.
[7] V. Sata, A. Sathonsaowaphak, P. Chindaprasirt, Resistance of lignite bottom ash geopolymer mortar to sulfate and sulfuric acid attack, Cem. Concr. Compos. 34 (2012) 700–708, https://doi.org/10.1016/J.CEMCONCOMP.2012.01.010.
[8] C. Grengg, F. Mittermayr, N. Ukrainczyk, G. Koraimann, S. Kienesberger, M. Dietzel, Advances in concrete materials for sewer systems affected by microbial induced concrete corrosion: a review, Water Res. 134 (2018) 341–352, https://doi.org/10.1016/j.watres.2018.01.043.
[9] J. Juhart, C. Gößler, C. Grengg, F. Mittermayr, O. Rudic, A. McIntosh, B. Freytag, Material characterization of geopolymer mortar for its beneficial use in composite construction, RILEM.Tech.Lett. 5 (2020) 174–185, https://doi.org/10.21809/RILEMTECHLETT.2020.125.
[10] T.T. Ngo, T.T. Tran, T.M. Pham, H. Hao, Performance of geopolymer concrete in monolithic and non-corrosive dry joints using CFRP bolts under cyclic loading, Compos. Struct. 258 (2021), 113394, https://doi.org/10.1016/J.COMPSTRUCT.2020.113394.
[11] A. Castel, S.J. Foster, T. Ng, J.G. Sanjayan, R.I. Gilbert, Creep and drying shrinkage of a blended slag and low calcium fly ash geopolymer Concrete, Mater. Struct./Materiaux et Construction 49 (2016) 1619–1628, https://doi.org/10.1617/S11527-015-0599-1.
[12] R. Si, Q. Dai, S. Guo, J. Wang, Mechanical property, nanopore structure and drying shrinkage of metakaolin-based geopolymer with waste glass powder, J. Clean. Prod. 242 (2020), 118502, https://doi.org/10.1016/J.JCLEPRO.2019.118502.
[13] M. Hojati, F. Rajabipour, A. Radlińska, Drying shrinkage of alkali activated fly ash: effect of activator composition and ambient relative humidity, in: Proceedings of the 4th International Conference on Sustainable Construction Materials and Technologies (SCMT4), Las Vegas, NV, USA, 2016, pp. 7–11.
[14] H. Ye, A. Radlińska, Shrinkage mechanisms of alkali-activated slag, Cement Concr. Res. 88 (2016) 126–135, https://doi.org/10.1016/j.cemconres.2016.07.001.
[15] G. Wang, Y. Ma, Drying Shrinkage of Alkali-Activated Fly Ash/slag Blended System, vol. 7, 2018, pp. 203–213, https://doi.org/10.1080/21650373.2018.1471424.
[16] Z. A.Li, J.Ye Liu, Drying Shrinkage of Alkali-Activated Slag and Fly Ash Concrete; A Comparative Study with Ordinary Portland Cement Concrete, 2019.
[17] P. Rovnaník, Effect of curing temperature on the development of hard structure of metakaolin-based geopolymer, Construct. Build. Mater. 24 (2010) 1176–1183, https://doi.org/10.1016/j.conbuildmat.2009.12.023.
[18] Z. Kubba, G. Fahim Huseien, A.R.M. Sam, K.W. Shah, M.A. Asaad, M. Ismail, M. M. Tahir, J. Mirza, Impact of curing temperatures and alkaline activators on compressive strength and porosity of ternary blended geopolymer mortars, Case Stud. Constr. Mater. 9 (2018), e00205, https://doi.org/10.1016/j.cscm.2018.e00205.
[19] P.K. Sarker, R. Haque, K.v. Ramgolam, Fracture behaviour of heat cured fly ash based geopolymer concrete, Mater. Des. 44 (2013) 580–586, https://doi.org/10.1016/j.matdes.2012.08.005.
[20] M.F. Nurruddin, H. Sani, B.S. Mohammed, I. Shaaban, Methods of curing geopolymer concrete: a review, Int. J.Adv.Appl. Sci. 5 (2018) 31–36, https://doi.org/10.21833/ijaas.2018.01.005.
[21] G. Görhan, R. Aslaner, O. Şinik, The effect of curing on the properties of metakaolin and fly ash-based geopolymer paste, Compos. B Eng. 97 (2016) 329–335, https://doi.org/10.1016/j.compositesb.2016.05.019.
[22] S.P. Singh, M. Murmu, Effects of curing temperature on strength of lime-activated slag cement, Int. J. Civ. Eng. 15 (2017) 575–584, https://doi.org/10.1007/S40999-017-0166-Y.
[23] A. Hasnaoui, E. Ghorbel, G. Wardeh, Effect of curing conditions on the performance of geopolymer concrete based on granulated blast furnace slag and metakaolin, J. Mater. Civ. Eng. 33 (2021), 04020501, https://doi.org/10.1061/(asce)mt.1943-5533.0003606.
[24] S. Chen, S. Ruan, Q. Zeng, Y. Liu, M. Zhang, Y. Tian, D. Yan, Pore structure of geopolymer materials and its correlations to engineering properties: a review,

Construct. Build. Mater. 328 (2022), 127064, https://doi.org/10.1016/J.CONBUILDMAT.2022.127064.
[25] Y. Ma, J. Hu, G. Ye, The pore structure and permeability of alkali activated fly ash, Fuel 104 (2013) 771–780, https://doi.org/10.1016/J.FUEL.2012.05.034.
[26] J.L. Provis, Alkali-activation of Calcined Clays – past, present and future, RILEM Bookseries 16 (2018) 372–376, https://doi.org/10.1007/978-94-024-1207-9_60.
[27] H. Abdulrahman, R. Muhamad, P. Visintin, A. Azim Shukri, Mechanical properties and bond stress-slip behaviour of fly ash geopolymer concrete, Construct. Build. Mater. 327 (2022), 126909, https://doi.org/10.1016/J.CONBUILDMAT.2022.126909.
[28] K.H. Mo, U.J. Alengaram, M.Z. Jumaat, Structural performance of reinforced geopolymer concrete members: a review, Construct. Build. Mater. 120 (2016) 251–264, https://doi.org/10.1016/J.CONBUILDMAT.2016.05.088.
[29] B.S. Hamad, A.A. Rteil, M. El-Fadel, Effect of used engine oil on properties of fresh and hardened concrete, Construct. Build. Mater. 17 (2003) 311–318, https://doi.org/10.1016/S0950-0618(03)00002-3.
[30] Y. Liu, Z. Yu, C. Lv, F. Meng, Y. Yang, Preparation of waste cooking oil emulsion as shrinkage reducing admixture and its potential use in high performance concrete: effect on shrinkage and mechanical properties, J. Build. Eng. 32 (2020), 101488, https://doi.org/10.1016/j.jobe.2020.101488.
[31] C. Nunes, Z. Slížková, Freezing and thawing resistance of aerial lime mortar with metakaolin and a traditional water-repellent admixture, Construct. Build. Mater. 114 (2016) 896–905, https://doi.org/10.1016/j.conbuildmat.2016.04.029.
[32] C. Reeb, C. Pierlot, C. Davy, D. Lambertin, Incorporation of organic liquids into geopolymer materials - a review of processing, properties and applications, Ceram. Int. 47 (2021) 7369–7385, https://doi.org/10.1016/J.CERAMINT.2020.11.239.
[33] C. Bai, G. Franchin, H. Elsayed, A. Conte, P. Colombo, High strength metakaolin-based geopolymer foams with variable macroporous structure, J. Eur. Ceram. Soc. 36 (2016) 4243–4249, https://doi.org/10.1016/J.JEURCERAMSOC.2016.06.045.
[34] R.M. Novais, R.C. Pullar, J.A. Labrincha, Geopolymer foams: an overview of recent advancements, Prog. Mater. Sci. 109 (2020), 100621, https://doi.org/10.1016/J.PMATSCI.2019.100621.
[35] J. Fiset, M. Cellier, P.Y. Vuillaume, Macroporous geopolymers designed for facile polymers post-infusion, Cem. Concr. Compos. 110 (2020), 103591, https://doi.org/10.1016/J.CEMCONCOMP.2020.103591.
[36] C. Bai, J. Zheng, G.A. Rizzi, P. Colombo, Low-temperature fabrication of SiC/geopolymer cellular composites, Compos. B Eng. 137 (2018) 23–30, https://doi.org/10.1016/J.COMPOSITESB.2017.11.013.
[37] EN 1015-3:2000/A2:2007 - European Standards, Methods of Test for Mortar for Masonry - Part 3: Determination of Consistence of Fresh Mortar (By Flow Table) - European Standards, 2007.
[38] EN 1015-11: 2007 - European Standards, Methods of Test for Mortar for Masonry-Part, vol. 11, 2007.
[39] EN 12390-6:2002 - European Standards, Testing Hardened Concrete–Tensile Splitting Strength of Test Specimens, 2002.
[40] ÖNORM 23303:2010 - Austrian Standards, Test Methods for Concrete-National Application of Testing Standards for Concrete and its Source Materials, 2010 (n.d.)).
[41] ÖNORM EN 1936:2007 02 01 - Austrian Standards, Natural Stone Test Methods - Determination of Real Density and Apparent Density, and of Total and Open Porosity, 2007.
[42] R. Snellings, J. Chwast, Ö. Cizer, N. de Belie, Y. Dhandapani, P. Durdzinski, J. Elsen, J. Haufe, D. Hooton, C. Patapy, M. Santhanam, K. Scrivener, D. Snoeck, L. Steger, S. Tongbo, A. Vollpracht, F. Winnefeld, B. Lothenbach, Report of TC 238-SCM: hydration stoppage methods for phase assemblage studies of blended cements—results of a round robin test, Mater. Struct./Materiaux et Construction 51 (2018) 1–12, https://doi.org/10.1617/S11527-018-1237-5.
[43] X. Chen, A. Meawad, L.J. Struble, Method to stop geopolymer reaction, J. Am. Ceram. Soc. 97 (2014) 3270–3275, https://doi.org/10.1111/JACE.13071.
[44] E.P. Barrett, L.G. Joyner, P.P. Halenda, The determination of pore volume and area distributions in porous substances. I. Computations from nitrogen isotherms, J. Am. Chem. Soc. 73 (1951) 373–380.
[45] S. Brunauer, P.H. Emmett, E. Teller, Adsorption of gases in multimolecular layers, J. Am. Chem. Soc. 60 (1938) 309–319.
[46] J. Zhu, R. Zhang, Y. Zhang, F. He, The fractal characteristics of pore size distribution in cement-based materials and its effect on gas permeability, Sci. Rep. 9 (2019) 1–12, https://doi.org/10.1038/s41598-019-53828-5, 2019 9:1.
[47] Fib model code for concrete structures 2010. https://doi.org/10.1002/9783433604090, 2013.
[48] S. Yoon, P.J.M. Monteiro, D.E. Macphee, F.P. Glasser, M.S.E. Imbabi, Statistical evaluation of the mechanical properties of high-volume class F fly ash concretes, Construct. Build. Mater. 54 (2014) 432–442, https://doi.org/10.1016/J.CONBUILDMAT.2013.12.077.
[49] N. de Belie, J. Kratky, S. van Vlierberghe, Influence of pozzolans and slag on the microstructure of partially carbonated cement paste by means of water vapour and nitrogen sorption experiments and BET calculations, Cement Concr. Res. 40 (2010) 1723–1733, https://doi.org/10.1016/J.CEMCONRES.2010.08.014.
[50] A. Noushini, M. Babaee, A. Castel, Suitability of heat-cured low-calcium fly ash-based geopolymer concrete for precast applications, Mag. Concr. Res. 68 (2015) 163–177, https://doi.org/10.1680/MACR.15.00065.
[51] C.K.B. Yip, The Role of Calcium in Geopolymerisation, PhD Thesis, University of Melbourne, 2004.
[52] D.P. Bentz, K.K. Hansen, H.D. Madsen, F. Vallée, E.J. Griesel, Drying/hydration in cement pastes during curing, Mater. Struct. 34 (2001) 557–565, https://doi.org/10.1007/BF02482182, 2001 34:9.
[53] A. Kirschner, H.H.- Ceramics-silikaty, Investigation of geopolymer binders with respect to their application for building materials, Ceramics-Silikaty.Cz. 48 (2004) (2004) 117–120. https://www.ceramics-silikaty.cz/2004/pdf/2004_03_117.pdf. (Accessed 31 July 2022).
[54] M. Safiuddin, S.N. Raman, M.F.M. Zain, Effect of different curing methods on the properties of microsilica concrete, Aust J Basic Appl Sci 1 (2007) 87–95.
[55] H. Ye, Creep mechanisms of calcium–silicate–hydrate: an overview of recent advances and challenges, Int J Concr Struct Mater 9 (2015) 453–462, https://doi.org/10.1007/S40069-015-0114-7.
[56] F. Puertas, T. Amat, A. Fernández-Jiménez, T. Vázquez, Mechanical and durable behaviour of alkaline cement mortars reinforced with polypropylene fibres, Cement Concr. Res. 33 (2003) 2031–2036, https://doi.org/10.1016/S0008-8846(03)00222-9.
[57] P. Nath, P.K. Sarker, Flexural strength and elastic modulus of ambient-cured blended low-calcium fly ash geopolymer concrete, Construct. Build. Mater. 130 (2017) 22–31, https://doi.org/10.1016/J.CONBUILDMAT.2016.11.034.
[58] P. Duxson, J.L. Provis, G.C. Lukey, S.W. Mallicoat, W.M. Kriven, J.S.J. van Deventer, Understanding the relationship between geopolymer composition, microstructure and mechanical properties, Colloids Surf. A Physicochem. Eng. Asp. 269 (2005) 47–58, https://doi.org/10.1016/J.COLSURFA.2005.06.060.
[59] T. da Silva Rocha, D.P. Dias, F.C.C. França, R.R. de Salles Guerra, L.R.D.C. de Oliveira Marques, Metakaolin-based geopolymer mortars with different alkaline activators (Na+ and K+), Construct. Build. Mater. 178 (2018) 453–461, https://doi.org/10.1016/J.CONBUILDMAT.2018.05.172.
[60] R.R. Bellum, K. Muniraj, C.S.R. Indukuri, S.R.C. Madduru, Investigation on performance enhancement of fly ash-GGBFS based graphene geopolymer concrete, J. Build. Eng. 32 (2020), 101659, https://doi.org/10.1016/J.JOBE.2020.101659.
[61] Z. Zhang, H. Wang, The pore characteristics of geopolymer foam concrete and their impact on the compressive strength and modulus, Front Mater 3 (2016) 38, https://doi.org/10.3389/FMATS.2016.00038.
[62] O. Linderoth, P. Johansson, L. Wadsö, Development of pore structure, moisture sorption and transport properties in fly ash blended cement-based materials, Construct. Build. Mater. 261 (2020), 120007, https://doi.org/10.1016/J.CONBUILDMAT.2020.120007.
[63] M. Saeidpour, L. Wadsö, Moisture equilibrium of cement based materials containing slag or silica fume and exposed to repeated sorption cycles, Cement Concr. Res. 69 (2015) 88–95, https://doi.org/10.1016/J.CEMCONRES.2014.12.005.
[64] O. Rudic, F. Mittermayr, N. Ukrainczyk, G. Gluth, S. Simon, Y. Seyrek, B. Freytag, J. Juhart, C. Grengg, On the Benefits of Vegetable Oil Addition for Alkali Activated Systems [Manuscript Submitted for Publication], 2023.
[65] P. Nath, P.K. Sarker, Flexural strength and elastic modulus of ambient-cured blended low-calcium fly ash geopolymer concrete, Construct. Build. Mater. 130 (2017) 22–31, https://doi.org/10.1016/J.CONBUILDMAT.2016.11.034.